Residue R216 and Catalytic Efficiency of a Murine Class Alpha Glutathione *S*-Transferase toward Benzo[*a*]pyrene 7(*R*),8(*S*)-Diol 9(*S*),10(*R*)-Epoxide[†,‡]

Yijun Gu,[§,||] Shivendra V. Singh,[§,⊥] and Xinhua Ji*[,||]

Program in Structural Biology, National Cancer Institute-Frederick Cancer Research and Development Center, Frederick, Maryland 21702, and Cancer Research Laboratory, Mercy Hospital of Pittsburgh, Pittsburgh, Pennsylvania 15219

Received June 19, 2000

ABSTRACT: Murine class alpha glutathione *S*-transferase A1-1 (mGSTA1-1), unlike mammalian class alpha GSTs, is the most efficient in the glutathione (GSH) conjugation of the ultimate carcinogenic metabolite of benzo[*a*]pyrene, (+)-*anti*-7,8-dihydroxy-9,10-oxy-7,8,9,10-tetrahydrobenzo[*a*]pyrene [(+)-*anti*-BPDE] [Hu, X., Srivastava, S. K., Xia, H., Awasthi, Y. C., and Singh, S. V. (1996) *J. Biol. Chem. 271*, 32684−32688]. Here, we report the crystal structures of mGSTA1-1 in complex with GSH and with the GSH conjugate of (+)-*anti*-BPDE (GSBpd) at 1.9 and 2.0 Å resolution, respectively. Both crystals belong to monoclinic space group *C*2 with one dimer in the asymmetric unit. The structures reveal that, within one subunit, the GSH moiety interacts with residues Y8, R14, K44, Q53, V54, Q66, and T67, whereas the hydrophobic moiety of GSBpd interacts with the side chains of F9, R14, M207, A215, R216, F219, and I221. In addition, the GSH moiety interacts with D100 and R130 from the other subunit across the dimer interface. The structural comparison between mGSTA1-1·GSH and mGSTA1-1·GSBpd reveals significant conformational differences. The movement of helix α9 brings the residues on the helix into direct interaction with the product. Most noticeable are the positional displacement and conformational change of R216, one of the residues located in helix α9. The side chain of R216, which points away from the H-site in the mGSTA1-1·GSH complex, probes into the active site and becomes parallel with the aromatic ring system of GSBpd. Moreover, the guanidinium group of R216 shifts ∼8 Å and forms a strong hydrogen bond with the C8 hydroxyl group of GSBpd, suggesting that the electrostatic assistance provided by the guanidinium group facilitates the ring-opening reaction of (+)-*anti*-BPDE. The structure of mGSTA1-1·GSBpd is also compared with those of hGSTP1-1[V104,A113]·GSBpd, hGSPA1-1·*S*-benzylglutathione, and mGSTA4-4·4-*S*-glutathionyl-5-pentyltetrahydrofuran-2-ol. The comparison provides further evidence that supports the functional roles of R216 and helix α9. The lack of mobility of helix α9 and/or the lack of electrostatic assistance from R216 may be responsible for the relatively lower activity of hGSTA1-1, mGSTA4-4, and hGSTP1-1 toward (+)-*anti*-BPDE.

Glutathione *S*-transferases (GSTs,[1] EC 2.5.1.18) catalyze the addition of the tripeptide thiol glutathione (GSH) to xenobiotic substrates that have an electrophilic functional group. The catalytic diversity of this family of detoxification enzymes arises, in part, from the existence of at least seven distinct gene classes: alpha, mu, pi, theta, sigma, kappa, and microsomal GSTs. Although GST isozymes of each class exhibit relatively broad substrate selectivity, most have unique catalytic attributes that are important in defining their physiological significance (*1*−*4*). The extent of understanding the precise enzyme−substrate interactions responsible for the catalytic properties has been greatly increased by the recent determinations of many three-dimensional structures of GSTs (for a review, see ref *5*). Both the GSH-binding site (G-site) and the xenobiotic substrate-binding site (H-site) are described in these crystal structures. The G-site is very well defined for the cytosolic GSTs, and three different GSH-binding modes have been observed, as summarized by Ji et al. (*6*). In contrast, the binding modes of xenobiotic substrates and product molecules are much more complex and class specific. For example, the H-site in rGSTM1-1 is a hydrophobic cavity (*7*), whereas in hGSTP1-1, it is half-hydrophobic and half-hydrophilic with functionally important water molecules (*6*, *8*).

GSTs are believed to play an important role in the cellular defense against the carcinogenic effects of polycyclic

[†] This work was supported in part by U.S. Public Health Service Grants R01 CA76348 and CA55589 (to S.V.S.) awarded by the National Cancer Institute.

[‡] The atomic coordinates and structure factors for the mGSTA1-1·GSH and mGSTA1-1·GSBpd complexes have been deposited with the Protein Data Bank under accession codes 1F3A and 1F3B.

* To whom correspondence should be addressed: NCI-FCRDC, Building 539, P.O. Box B, Frederick, MD 21702. Phone: (301) 846-5035. Fax: (301) 846-6073. E-mail: jix@ncifcrf.gov.

[§] Mercy Hospital of Pittsburgh.

[||] National Cancer Institute-Frederick Cancer Research and Development Center.

[⊥] Current address: University of Pittsburgh, Pittsburgh, PA 15213.

[1] Abbreviations: GSH, glutathione; GST, GSH *S*-transferase; xGSTY*m*-*n*, class Y (A, alpha; M, mu; P, pi; T, theta; S, sigma; K, kappa) GST with subunit type *m*-*n* (*m* and *n* = 1, 2, ...) from x (m, murine; h, human; r, rat; s, squid; b, bovine); BP, benzo[*a*]pyrene; (+)-*anti*-BPDE, (+)-*anti*-7,8-dihydroxy-9,10-oxy-7,8,9,10-tetrahydrobenzo-[*a*]pyrene; GSBpd, GSH conjugate of (+)-*anti*-BPDE; GSHna, 4-*S*-glutathionyl-5-pentyltetrahydrofuran-2-ol; GSBen, *S*-benzylglutathione; G-site, GSH-binding site; H-site, xenobiotic substrate-binding site; PAH, polycyclic aromatic hydrocarbon; rms, root-mean-square.

10.1021/bi001396u CCC: $19.00 © 2000 American Chemical Society
Published on Web 09/20/2000

hydrocarbons (PAHs), which are widespread environmental pollutants (*9*). The mutagenic and carcinogenic activities of many PAHs, including the prototypical member benzo[*a*]-pyrene (BP), are attributed to their respective diol epoxides (*10*−*12*), which are substrates for GSTs (*13*−*17*). The GST isozymes of various classes differ remarkably in their activity toward PAH diol epoxides (*13*−*17*). For example, previous studies with purified human and rat GST isozymes have shown that the class pi isozyme is relatively more efficient than other classes of GSTs in the GSH conjugation of (+)-*anti*-7,8-dihydroxy-9,10-oxy-7,8,9,10-tetrahydrobenzo[*a*]pyrene [(+)-*anti*-BPDE] (*13*, *14*), which is the ultimate carcinogenic metabolite of BP (*11*, *12*). These studies have also shown that (+)-*anti*-BPDE is a poor substrate for class alpha rat and human GSTs (*13*−*15*). More recently, we have demonstrated that mGSTA1-1, which is a class alpha murine GST isozyme, is the most efficient in the GSH conjugation of (+)-*anti*-BPDE (*18*). The catalytic efficiency of mGSTA1-1 is approximately 3.3−655-fold higher than that of mGSTA2-2, mGSTP1-1, mGSTA3-3, mGSTM1-1, or mGSTA4-4 (*18*−*20*). Moreover, the catalytic efficiency of mGSTA1-1 is approximately 4.5-fold higher than that of hGSTP1-1, which among human GSTs is most efficient in the GSH conjugation of (+)-*anti*-BPDE (*14*). To elucidate the structure and relatively higher catalytic efficiency of mGSTA1-1 toward (+)-*anti*-BPDE, we have determined the crystal structures of mGSTA1-1 in complex with GSH and with the GSH conjugate of (+)-*anti*-BPDE (GSBpd).

EXPERIMENTAL PROCEDURES

Crystallization and X-ray Diffraction Data Collection. mGSTA1-1 was expressed and purified as described previously (*19*, *20*). GSBpd was synthesized and purified as reported elsewhere (*18*). The hanging drop vapor diffusion technique was used to grow both complex crystals. For the mGSTA1-1·GSH complex, the initial drop contained 3.7% mGSTA1-1, 7.5% PEG 4000, and 3.75% 2-propanol in 37 mM Na/HEPES (pH 7.5). The drops were equilibrated at 15 °C against the well solution [7.5% 2-propanol, 15% PEG 4000, and 75 mM HEPES (pH 7.5)]. Diffraction-quality crystals were grown within 2 days. The cryoprotectant was composed of 15% glycerol, 17% PEG 4000, and 8.5% 2-propanol in 85 mM HEPES (pH 7.5). For the mGSTA1-1·GSBpd complex, similar conditions were used except that 2.6 mM GSBpd was present in the drops.

X-ray diffraction data were collected from single crystals at beamline X9B of the National Synchrotron Light Source at Brookhaven National Laboratory (Upton, NY). Crystals were flash-frozen and were kept frozen at 100 K. A CCD detector was employed in all data collection runs. The raw data images were processed and scaled using Denzo and Scalepack (*21*). Data collection statistics are summarized in Table 1.

Crystal Structure Determination and Refinement. The structure of the mGSTA1-1·GSBpd complex was determined by molecular replacement using the program AmoRe (*22*). The search model was one subunit of the crystal structure of the dimeric mGSTA2-2·GSH[2] complex with all the water molecules excluded. The rotation function was calculated using data within the resolution range of 10−4 Å. The rotational search resulted in two outstanding peaks; the higher peak had a correlation coefficient of 0.234. After the translational search for the first solution, the second solution was obtained with the first solution fixed. The correlation coefficient was 0.55, and the crystallographic *R*-factor was 0.41 for both subunits. Rigid-body refinement within AmoRe improved the correlation coefficient to 0.701 and the crystallographic *R*-factor to 0.34. The structure of the mGSTA1-1·GSH complex was determined by the difference Fourier technique, using the refined mGSTA1-1·GSBpd structure as the starting model with the GSBpd and solvent molecules excluded.

Table 1: Summary of Data Collection for the mGSTA1-1·GSBpd and mGSTA1-1·GSH Complexes

	mGSTA1-1·GSBpd	mGSTA1-1·GSH
wavelength (Å)	1.01	0.92
space group	*C*2	*C*2
unit cell parameters		
a (Å)	99.08	99.30
b (Å)	93.19	93.64
c (Å)	51.94	52.22
β (deg)	91.75	91.80
resolution (Å)	40.0−2.0	30.0−1.9
redundancy	3.15	3.71
overall completeness (%)	98.6	98.0
last shell completeness (%)[a]	97.5	93.8
overall $I/\sigma(I)$	9.05	15.7
last shell $I/\sigma(I)$[a]	2.42	2.90
$R_{scaling}$[b]	0.133	0.075

[a] Values of 2.07−2.00 Å for the mGSTA1-1·GSBpd complex and 1.97−1.90 Å for the mGSTA1-1·GSH complex. [b] $R_{scaling} = \Sigma|I - \langle I\rangle|/\Sigma I$. Friedel pairs were merged.

The crystal structure refinement was initiated with the X-PLOR 3.851 package (*23*). A total of 5% reflections were randomly chosen for the R_{free} calculations. Global energy crystallographic refinement and individual *B*-factor refinement were employed. Very strict noncrystallographic restraints were applied for the two subunits of the dimeric molecule. The starting model of the mGSTA1-1·GSBpd complex had the uniformly assigned temperature factor of 20.0 Å^2, and the first round of refinement resulted in an R_{free} of 0.38 and an *R*-factor of 0.34 for reflections of 10.0−2.2 Å with an $I/\sigma(I)$ of 2. Maps with $2F_o - F_c$ and $F_o - F_c$ Fourier coefficients were calculated, which revealed the position of GSBpd in both subunits. The whole model was checked and adjusted against the electron density maps and the primary amino acid sequence of mGSTA1-1. Residues with incomplete density were replaced with alanine or glycine, which were mainly located in the C-terminal helix starting from M207. No density was found for residues 221 and 222. The weight for the noncrystallographic restraints was gradually reduced along with the refinement. After four rounds of refinement, the R_{free} and *R*-factor dropped to 0.33 and 0.29, respectively. The electron density was well-defined except for the last portion of the polypeptide chain. Water molecules were picked up from the difference Fourier maps as peaks higher than 3.0σ, and the data for refinement were progressively extended to 2.2 Å. Simulated annealing omit maps were calculated to locate and verify the positions of C-terminal residues. After eight rounds of refinement with X-PLOR 3.851, the R_{free} and *R*-factor dropped to 0.31 and 0.26, respectively. The refinement was continued using the

[2] Y. Gu, S. V. Singh, and X. Ji, unpublished results.

Table 2: Summary of Refinement Statistics for the mGSTA1-1·GSBpd and mGSTA1-1·GSH Complexes

	mGSTA1-1·GSBpd	mGSTA1-1·GSH
resolution range (Å)	40.0−2.0	30.0−1.9
no. of reflections with an $I/\sigma(I)$ of 1	31149	36861
working set for refinement	29606	34998
test set for R_{free} calculation	1543	1863
R-factor (%)[a]	17.6	19.1
R_{free} (%)	23.4	24.8
no. of protein atoms	3584	3546
no. of ligand molecules	2 GSBpd	2 GSH
no. of water molecules	523	450
rms deviations from ideal geometry		
bond distances (Å)	0.014	0.015
bond angles (deg)	1.60	1.75

[a] Crystallographic R-factor $= \Sigma_{hkl}||F_o| - |F_c||/\Sigma_{hkl}|F_o|$.

program suite CNS_0.4 (*23*), using the maximum likelihood target function and data within 20.0−2.0 Å with bulk solvent correction. The weight of noncrystallographic restraints was dropped to 0 in a few steps. After a total of 37 rounds of refinement, the density of residues 207−221 in both subunits was significantly improved. The R_{free} and R-factor for the final model were 0.234 and 0.176, respectively, for reflections within 40.0−2.0 Å with an $I/\sigma(I)$ of 1. The two subunits contain 3584 protein atoms, 2 GSBpd molecules, and 523 oxygen atoms of water molecules. The same strategy was applied in the refinement of the mGSTA1-1·GSH structure. The R_{free} and R-factor for the final model were 0.248 and 0.191, respectively, for reflections within 30.0−1.9 Å with an $I/\sigma(I)$ of 1 (Table 2). The final model is a dimer, containing 3546 protein atoms, 2 GSH molecules, and 450 water molecules. In the refinement of both structures, all identifiable water molecules were verified by a series of omit maps (*24*) with a set of 100 molecules deleted each time. All X-ray diffraction data were included in electron density map calculations, and the program suite O (*25*) was used to check and modify models and to add and delete water molecules. A detailed summary of the crystallographic refinement is shown in Table 2.

RESULTS AND DISCUSSION

Overall Structure. The final structures have good geometry with reasonable root-mean-square (rms) deviations for bond lengths and bond angles (Table 2). As revealed by the protein structure validation program PROCHECK (*26*), more than 90% of the residues in both structures exhibit the most favorable $\phi-\varphi$ relationship and no residue has disallowed $\phi-\varphi$ relationships. The overall structure of the mGSTA1-1·GSBpd complex is schematically illustrated in Figure 1a. There is one dimer in the asymmetric unit, and both GSBpd molecules have well-defined electron density (for example, see Figure 1b). Each subunit is composed of nine α-helices and four β-strands, which are organized into two domains. The smaller N-terminal domain contains the secondary-structure elements β2, α1, β1, α2, β3, β4, and α3, and the larger C-terminal domain contains six α-helices (Figure 1a). The overall, subunit, and domain structures are very similar to those of other class alpha GSTs, such as hGSTA1-1 (*27*) and mGSTA4-4 (*28*).

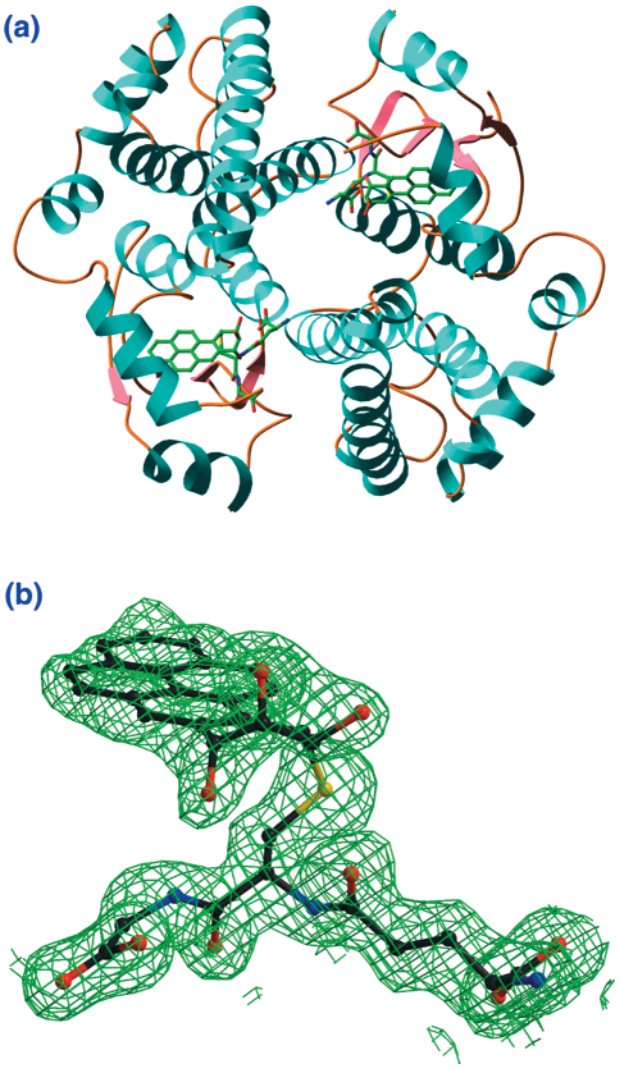

FIGURE 1: Overall structure of the mGSTA1-1·GSBpd complex. (a) Schematic representation of the dimeric mGSTA1-1·GSBpd complex. Each molecule contains nine α-helices (cyan), four β-strands (dark pink), and one product molecule (GSBpd, green). The view is along the pseudo-2-fold axis. The figure was prepared with the program RIBBOBS (*34*). (b) Typical $2F_o - F_c$ electron density (green net) contoured at 1.0σ around the GSBpd molecule, which is shown as a ball-and-stick model with the atomic color scheme (carbon in black, oxygen in red, nitrogen in blue, and sulfur in yellow). The illustration was prepared with the program MOLSCRIPT (*35*).

Active Center and GSBpd Binding in mGSTA1-1. In both subunits of the mGSTA1-1·GSH complex as well as those of the mGSTA1-1·GSBpd complex, the GSH moiety is bound to the G-site via comprehensive electrostatic interactions. Most of the polar atoms in GSH are involved in the formation of hydrogen bonds and/or salt bridges (*27*), among which the hydrogen bond between atom SG2 of GSH and atom OH of Y8 is shown in Figure 2. The H-site in mGSTA1-1 is composed of conserved residues Y8, F9, and R14 and C-terminal residues M207, A215, F219, and I221. These hydrophobic side chains construct a hydrophobic pocket for the binding of xenobiotic substrates such as (+)-*anti*-BPDE (Figure 1). The binding of the BPDE moiety of GSBpd in the active center is shown in Figure 2. The contact between the BPDE moiety and the H-site residues includes both electrostatic and hydrophobic interactions. There are

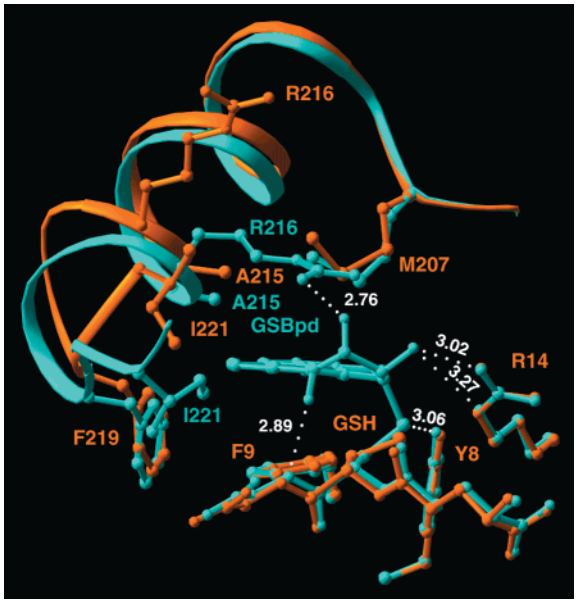

FIGURE 2: Significant conformational changes of the H-site in mGSTA1-1 upon xenobiotic substrate binding as revealed by the comparison of mGSTA1-1·GSH (orange) and mGSTA1-1·GSBpd (blue) complexes. The side chains are represented as ball-and-stick models, and the electrostatic interactions are illustrated as dotted white lines.

three hydroxyl groups on the BPDE moiety, among which the C7 hydroxyl forms a hydrogen bond with N3 of the GSH moiety, whereas those of C8 and C9 form hydrogen bonds with R216 and R14, respectively (Figure 2). Previously, it has been demonstrated that R14 is indeed a catalytic residue in various GST isozymes. We found, in the present study, that R216 from the C-terminal helix interacts with the product and/or substrate molecule(s). It appears that R216 has two roles in catalysis: participating in the binding of the substrate, intermediate, and/or product molecule(s) and providing electrostatic assistance in the epoxide ring-opening reaction. As shown in Figure 2, the BPDE moiety is sandwiched between the hydrophobic portion of the R216 side chain and the phenyl ring system of F9. The distance from the F9 phenyl ring to the BPDE polycyclic aromatic system is 4.0 Å, and that from BPDE to the R216 side chain is 3.8 Å. In addition, the BPDE moiety is surrounded by the hydrophobic side chains of M207, A215, F219, and I221 with contact distances of 4.5, 3.9, 3.5, and 3.5 Å, respectively. Among the side chains interacting with the BPDE moiety of GSBpd, those of R216 and I221 exhibit the largest conformational changes upon substrate or product binding (Figure 2).

Xenobiotic-Induced Conformational Changes in mGSTA1-1. The unique C-terminus of class alpha GSTs plays important roles in catalysis and, therefore, has been recognized as the critical component of the active site (*27*, *29*). The active site of mGSTA1-1 exerts significant conformational changes upon the binding of GSBpd (Figure 2). First, the C-terminal α9 helix moves toward the H-site. Second, along with the shift of the C-terminal helix, the Cα atom of R216 moves ~2.3 Å and the side chain shifts from pointing away from the H-site to protruding into the active center. The guanidinium group of R216 moves ~7.7 Å and forms a strong hydrogen bond (2.76 Å) with the C8 hydroxyl group of BPDE (Figure 2). This electrostatic interaction may serve to orient and position the substrate (+)-*anti*-BPDE in the H-site and also to facilitate the ring-opening reaction of the epoxide. Third, in the mGSTA1-1·GSH complex, I221 is partially disordered and Q222 is completely disordered, whereas in the mGSTA1-1·GSBpd complex, both I221 and Q222 are well-defined. The ϕ and φ angles of K220 in the mGSTA1-1·GSH complex are −99° and 114°, respectively, whereas in the mGSTA1-1·GSBpd complex, they are 48° and 97°, respectively. Consequently, I221 exhibits significant positional changes upon xenobiotic binding and interacts extensively with the bound substrate (Figure 2).

H-Site Comparison of mGSTA1-1 with hGSTA1-1. hGSTA1-1 is abundant in human liver and kidney (*3*). However, it has very low catalytic efficiency in the GSH conjugation of (+)-*anti*-BPDE (*15*) compared with mGSTA1-1 (*19*, *20*). The amino acid sequences of isozymes hGSTA1-1 and mGSTA1-1 are 75.1% identical, and they have similar three-dimensional folds. In the hGSTA1-1 structure, the H-site is composed of hydrophobic residues F9, R14, M207, A215, A218, F219, and F221, among which four are located in the C-terminal helix (Figure 3a, A215 and A218 not shown). When compared with the H-site in mGSTA1-1, however, the C-terminal helix appears to squeeze into the H-site and is probably kept in this position by the salt bridge between R220 and D41 (Figure 3a). Consequently, the H-site of hGSTA1-1 is too narrow to accommodate the bulky (+)-*anti*-BPDE. The unavailability of R216 and the narrow H-site are probably responsible for the very low catalytic efficiency of hGSTA1-1 toward (+)-*anti*-BPDE (*15*).

H-Site Comparison of mGSTA1-1 and mGSTA4-4. mGSTA4-4, which is another murine class alpha GST isozyme (*3*), exhibits high activity in conjugating the lipid peroxidation product 4-hydroxynon-2-enal with GSH (*30*). However, (+)-*anti*-BPDE is a very poor substrate for this isozyme (*18*). The sequences of isozymes mGSTA4-4 and mGSTA1-1 are 64.3% identical, and they have very similar three-dimensional structures (this work and ref *28*). In addition, R14 is available in both mGSTA1-1 (this work) and mGSTA4-4 (*28*) for catalysis. A closer examination of the two structures reveals that two additional proline residues in mGSTA4-4, P207 and P210, may contribute to its low activity toward (+)-*anti*-BPDE (Figure 3b). The residue corresponding to P207 in mGSTA1-1 is M207, which has been proven to be very important in catalysis by both structural analysis (this work) and kinetic analysis of site-directed mutants (*20*). The change of M207 to P207 results in three consecutive proline residues (P205, P206, and P207) and thereby alters the flexibility of the loop before the C-terminal helix. Residue K210 in mGSTA1-1 corresponds to P210 in mGSTA4-4, which is located at the N-terminus of the C-terminal helix and thereby alters the direction of the C-terminal helix (Figure 3b). Consequently, R216, which is important in (+)-*anti*-BPDE catalysis, is blocked by V215 (Figure 3b) and F110 (not shown in Figure 3b), and therefore, it is impossible for R216 to reach the active center of mGSTA4-4.

H-Site Comparison of mGSTA1-1 and hGSTP1-1. The class pi isozyme hGSTP1-1 is overexpressed in preneoplastic and tumor tissues and is believed to contribute to human cell resistance to alkylating agents (*31*, *32*). Moreover, this isozyme is also important in the metabolism and detoxification of many carcinogenic xenobiotics in humans (*3*, *17*, *33*). The catalytic efficiency of hGSTP1-1 toward (+)-*anti*-

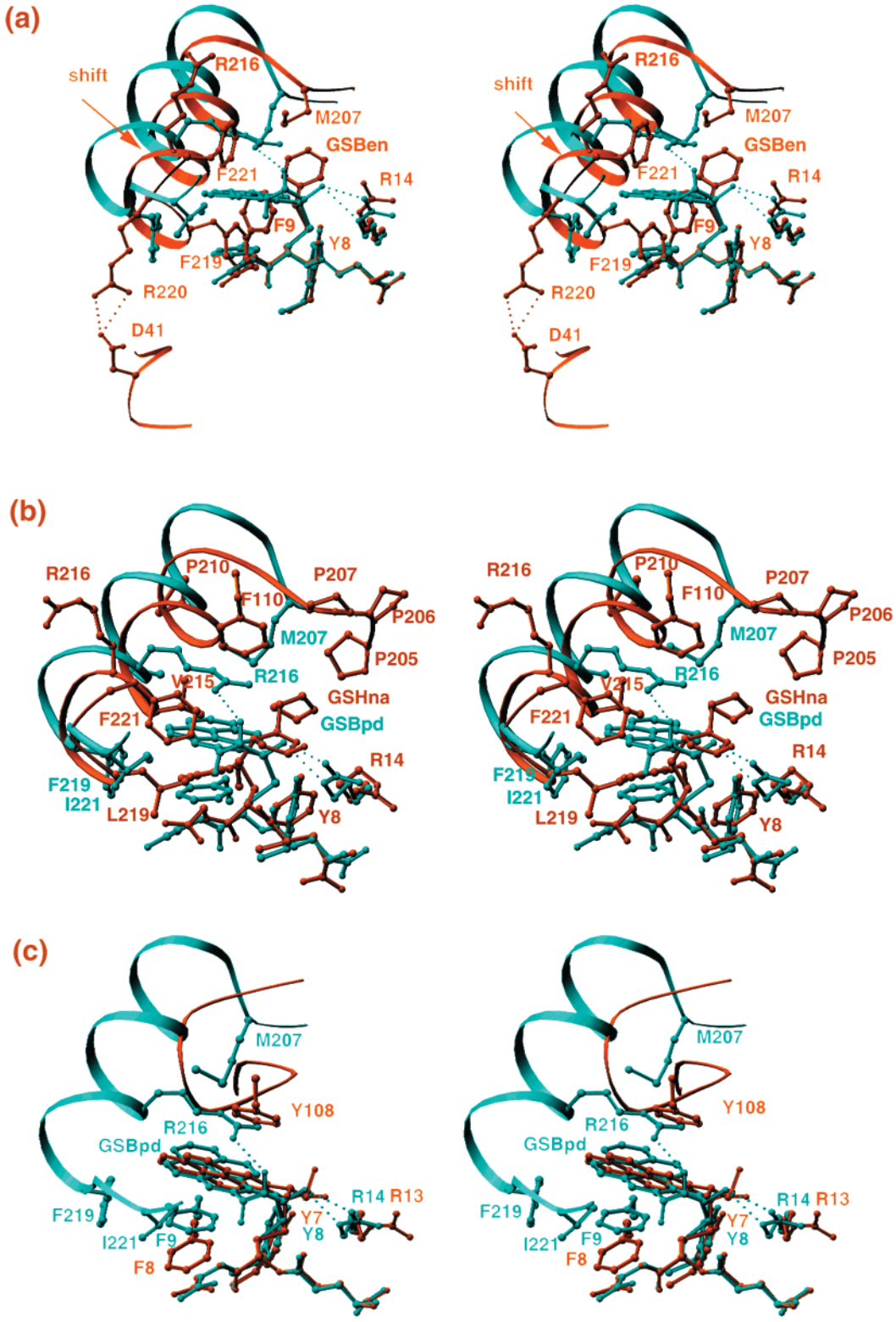

FIGURE 3: H-Site comparison of mGSTA1-1 (blue) with (a) hGSTA1-1 (orange), suggesting that the salt bridge between R220 and D41 in hGSTA1-1 is responsible for the low mobility of the C-terminal helix and, therefore, the squeezed H-site; (b) mGSTA4-4 (orange), indicating that P205, P206, P207, and P210 in mGSTA4-4 may be responsible for the rigidity of its C-terminal helix and, therefore, the narrow H-site; and (c) hGSTP1-1 (orange), implying that the Y108R mutant of hGSTP1-1 has an improved catalytic efficiency toward (+)-*anti*-BPDE. The illustration was prepared with RIBBONS (*34*).

BPDE, however, is about 4.5-fold lower than that of mGSTA1-1 (*14*, *18*). Figure 3c depicts the active site differences between the structures of mGSTA1-1 and hGSTP1-1, both of which are in complex with GSBpd. The comparison reveals the following differences. First, the C-terminal helix in mGSTA1-1 is not present in hGSTP1-1; therefore, residues A215 (not shown in Figure 3c), R216, and I221 are not available to interact with the bound xenobiotic substrates. Second, the BPDE moiety in the mGSTA1-1·GSBpd complex is sandwiched between the F8

and R216 side chains, whereas it is between the F9 side chain and the G205 backbone (not shown) in the hGSTP1-1·GSBpd complex. Third, the guanidinium group of R216 in mGSTA1-1 forms a hydrogen bond with the C8 hydroxyl group of BPDE, whereas in hGSTP1-1, the Y108 hydroxyl may provide electrostatic assistance in the addition of GSH to the epoxide (*6*). Although in the three-dimensional structure the R216 guanidinium group in mGSTA1-1 and the Y108 hydroxyl group in hGSTP1-1 fall into the same area, the difference in the charge of the two side chains may result in significant differences in catalysis, given that the assistance provided by this residue is of an electrostatic nature. Molecular modeling has shown that the Y108R mutant of hGSTP1-1 may be able to offer stronger electrostatic assistance to the ring-opening reaction and, therefore, may have improved activity toward (+)-*anti*-BPDE.

ACKNOWLEDGMENT

We thank Dr. Hong Xia for the purification of mGSTA1-1 and Dr. Zbigniew Dauter for his assistance and advice during the X-ray data acquisition at synchrotron beamline X9B at the Brookhaven National Laboratory.

REFERENCES

1. Armstrong, R. N. (1991) *Chem. Res. Toxicol. 4*, 131−140.
2. Armstrong, R. N. (1994) *Adv. Enzymol. Relat. Areas Mol. Biol. 69*, 1−44.
3. Hayes, J. D., and Pulford, D. J. (1995) *Crit. Rev. Biochem. Mol. Biol. 30*, 445−600.
4. Armstrong, R. N. (1997) *Chem. Res. Toxicol. 10*, 2−18.
5. Dirr, H., Reinemer, P., and Huber, R. (1994) *Eur. J. Biochem. 220*, 645−661.
6. Ji, X., Tordova, M., O'Donnell, R., Parsons, J. F., Hayden, J. B., Gilliland, G. L., and Zimniak, P. (1997) *Biochemistry 36*, 9690−9702.
7. Ji, X., Johnson, W. W., Sesay, M. A., Dickert, L., Prasad, S. M., Ammon, H. L., Armstrong, R. N., and Gilliland, G. L. (1994) *Biochemistry 33*, 1043−1052.
8. Ji, X., Blaszczyk, J., Xiao, B., O'Donnell, R., Hu, X., Herzog, C., Singh, S. V., and Zimniak, P. (1999) *Biochemistry 38*, 10231−10238.
9. Cancer, I. A. f. R. o. (1973) *IARC Monograph on the Evaluation of Carcinogenic Risk of Chemicals to Man*, Vol. 3, International Agency for Research on Cancer, Lyon, France.
10. Thakker, D. R., Yagi, H., Levin, W., Wood, A. W., Conney, A. H., and Jerina, D. M. (1985) in *Bioactivation of Foreign Compounds* (Anders, M. W., Ed.) pp 177−242, Academic Press, New York.
11. Buening, M. K., Wislocki, P. G., Levin, W., Yagi, H., Thakker, D. R., Akagi, H., Koreeda, M., Jerina, D. M., and Conney, A. H. (1978) *Proc. Natl. Acad. Sci. U.S.A. 75*, 5358−5361.
12. Slaga, T. J., Bracken, W. J., Gleason, G., Levin, W., Yagi, H., Jerina, D. M., and Conney, A. H. (1979) *Cancer Res. 39*, 67−71.
13. Robertson, I. G., Jensson, H., Mannervik, B., and Jernstrom, B. (1986) *Carcinogenesis 7*, 295−299.
14. Robertson, I. G., Guthenberg, C., Mannervik, B., and Jernstrom, B. (1986) *Cancer Res. 46*, 2220−2224.
15. Jernstrom, B., Funk, M., Frank, H., Mannervik, B., and Seidel, A. (1996) *Carcinogenesis 17*, 1491−1498.
16. Sundberg, K., Widersten, M., Seidel, A., Mannervik, B., and Jernstrom, B. (1997) *Chem. Res. Toxicol. 10*, 1221−1227.
17. Hu, X., Xia, H., Srivastava, S. K., Pal, A., Awasthi, Y. C., Zimniak, P., and Singh, S. V. (1998) *Cancer Res. 58*, 5340−5343.
18. Hu, X., Srivastava, S. K., Xia, H., Awasthi, Y. C., and Singh, S. V. (1996) *J. Biol. Chem. 271*, 32684−32688.
19. Xia, H., Pan, S. S., Hu, X., Srivastava, S. K., Pal, A., and Singh, S. V. (1998) *Arch. Biochem. Biophys. 353*, 337−348.
20. Xia, H., Gu, Y., Pan, S. S., Ji, X., and Singh, S. V. (1999) *Biochemistry 38*, 9824−9830.
21. Otwinowski, Z., and Minor, W. (1997) *Methods Enzymol. 276*, 307−326.
22. Navaza, J. (1994) *Acta Crystallogr. A50*, 157−163.
23. Brünger, A. T., and Rice, L. M. (1997) *Methods Enzymol. 277*, 243−269.
24. Bhat, T. N. (1988) *J. Appl. Crystallogr. 21*, 279−281.
25. Jones, T. A., and Kjeldgaard, M. (1997) *Methods Enzymol. 277*, 173−208.
26. Laskowski, R. A., MacArthur, M. W., Moss, D. S., and Thornton, J. M. (1993) *J. Appl. Crystallogr. 26*, 283−291.
27. Sinning, I., Kleywegt, G. J., Cowan, S. W., Reinemer, P., Dirr, H. W., Huber, R., Gilliland, G. L., Armstrong, R. N., Ji, X., Board, P. G., Olin, B., Mannervik, B., and Jones, T. A. (1993) *J. Mol. Biol. 232*, 192−212.
28. Xiao, B., Singh, S. P., Awasthi, Y. C., Zimniak, P., and Ji, X. (1999) *Biochemistry 38*, 11887−11894.
29. Cameron, A. D., Sinning, I., L'Hermite, G., Olin, B., Board, P. G., Mannervik, B., and Jones, T. A. (1995) *Structure 3*, 717−727.
30. Zimniak, P., Eckles, M. A., Saxena, M., and Awasthi, Y. C. (1992) *FEBS Lett. 313*, 173−176.
31. Tsuchida, S., and Sato, K. (1992) *Crit. Rev. Biochem. Mol. Biol. 27*, 337−384.
32. Waxman, D. J. (1990) *Cancer Res. 50*, 6449−6454.
33. Hu, X., O'Donnell, R., Srivastava, S. K., Xia, H., Zimniak, P., Nanduri, B., Bleicher, R. J., Awasthi, S., Awasthi, Y. C., Ji, X., and Singh, S. V. (1997) *Biochem. Biophys. Res. Commun. 235*, 424−428.
34. Carson, M. (1987) *J. Mol. Graphics 5*, 103−106.
35. Kraulis, P. J. (1991) *J. Appl. Crystallogr. 24*, 946−950.

BI001396U